

Critical Scaling of Compression-Driven Jamming of Frictionless Spheres

Anton Peshkov¹ and S. Teitel¹

¹*Department of Physics and Astronomy, University of Rochester, Rochester, NY 14627*

(Dated: December 22, 2024)

We numerically study the jamming transition of athermal, overdamped, frictionless spheres in two and three dimensions, compressed isotropically at a fixed rate $\dot{\gamma}$. The finite compression rate introduces a control time scale, which allows one to probe the critical time scale associated with jamming. As was found previously for steady-state shear-driven jamming, we find for compression-driven jamming that pressure obeys a critical scaling relation as a function of packing fraction ϕ and compression rate $\dot{\gamma}$, and that the bulk viscosity $p/\dot{\gamma}$ diverges upon jamming. A scaling analysis determines the critical exponents associated with the compression-driven jamming transition. Our results suggest that stress-isotropic, compression-driven, jamming may be in the same universality class as stress-anisotropic, shear-driven, jamming.

Athermal granular and related soft matter materials, such as non-Brownian suspensions, emulsions, and foams, all undergo a phase transition from a liquid-like state to a rigid disordered state as the packing fraction ϕ of the granular particles increases. This is the jamming transition [1, 3]. Here we focus on the behavior of frictionless particles, where jamming behaves like a continuous phase transition. Early studies of jamming focused on what we will call stress-isotropic jamming: mechanically stable jammed configurations are generated by isotropically compressing the system, or by energy quenching random initial configurations at fixed ϕ [2–4]. At low ϕ particles avoid each other and the pressure p vanishes. At a critical ϕ_J a system spanning rigid cluster forms and the pressure becomes finite, while the shear stress σ remains zero. Later studies investigated shear-driven jamming [6–15], where the system is uniformly sheared at a fixed strain rate $\dot{\gamma}$. For systems with a Newtonian rheology, such as particles in suspension, the system flows at low ϕ and small $\dot{\gamma}$ with a shear stress $\sigma \propto \dot{\gamma}$. Thus, for $\dot{\gamma} \rightarrow 0$, the viscosity $\eta = \sigma/\dot{\gamma}$ remains finite. However, above a critical ϕ_J , the system develops a non-zero yield stress $\sigma_0(\phi) = \lim_{\dot{\gamma} \rightarrow 0} \sigma > 0$ leading to a diverging viscosity. Because of this finite σ , we will refer to this as stress-anisotropic jamming. Given the different symmetry of anisotropic shear-driven jamming vs isotropic compression-driven jamming, it is natural to wonder if they belong to the same critical universality class.

A mean-field calculation in the limit of infinite dimensions [16], applying a shear stress within mechanically stable jammed states above ϕ_J until the system yields, found that critical exponents describing the inter-particle force distribution and gap distances in the sheared states were the same as predicted for isotropically jammed configurations. Subsequent numerical works [17, 18] in three dimensions supported this conclusion. However these works concern the structural properties of static stress-anisotropic states, rather than the dynamic behavior of driven steady states as in the shear-driven jamming described above. They thus do not probe the time scale associated with the jamming.

This time scale was considered in a recent numerical work by Ikeda et al. [19]. In contrast to many previous works, which used rapid energy minimizations to find jammed configurations, Ikeda et al. let their configurations relax according to equations of motion that incorporate the forces acting on the particles. For configurations below jamming, $\phi < \phi_J$, they measured the decay time τ of relaxation to zero energy. For random, stress-isotropic, initial configurations, they found τ to be governed by a unique isolated frequency mode, as was previously found for uniformly sheared systems [6]. As $\phi \rightarrow \phi_J$ from below, this τ diverged algebraically with a critical exponent consistent with that found by Olsson [8] for the relaxation of stress-anisotropic sheared steady states. In the latter case it was shown that τ scales proportional to the shear viscosity η . This suggests that isotropic and anisotropic jamming are in the same universality class. However, in a more recent work [1], several of the same authors of [19], question their previous result and claim that the relaxation time τ diverges logarithmically with the number of particles in the system for any $\phi < \phi_J$; thus τ has no proper thermodynamic limit.

Here we take a different approach to probing the time scale of isotropic jamming, by isotropically compressing at a finite rate in both two (2D) and three (3D) dimensions. Previous studies of compression-driven jamming generally focused on quasistatic compression [2–4]. In contrast, compression at a finite rate $\dot{\gamma}$ introduces a control time scale. By varying $\dot{\gamma}$ one can probe the critical time scale associated with jamming. Compression at a finite rate has previously been considered in [23, 24], however they considered inertial hard spheres with elastic collisions and an initial velocity distribution sampled at a finite temperature, as might describe a thermal glass; they also did not investigate the critical behavior. Here we consider the compression of soft-core, overdamped, athermal spheres, as in a non-Brownian suspension. We measure both the pressure p and the bulk viscosity $\zeta \equiv p/\dot{\gamma}$, finding that ζ has a well defined limit below jamming as $\dot{\gamma} \rightarrow 0$. We create an ensemble of states by compressing several independent random initial configurations from

a low ϕ_{init} up through the jamming ϕ_J , using differing compression rates $\dot{\gamma}$. We analyze the results using a critical scaling ansatz, just as has been done for shear-driven jamming [7, 8]. Considering soft spheres allows us to measure not only how ζ behaves below ϕ_J , but also how p behaves above ϕ_J . We find behavior qualitatively the same as for shear-driven jamming, with p vanishing as $\phi \rightarrow \phi_J$ from above, and ζ diverging as $\phi \rightarrow \phi_J$ from below. This establishes the presence of a well defined, diverging, time scale for isotropic jamming. A scaling analysis then strongly suggests that the critical exponents in 2D are the same as previously found for shear-driven jamming; the situation in 3D remains less clear.

Model: Our model consists of bidisperse, frictionless, soft-core spheres, with equal numbers of big and small spheres with diameter ratio $d_b/d_s = 1.4$ [3]. For particles with center of mass positions \mathbf{r}_i , and $r_{ij} = |\mathbf{r}_i - \mathbf{r}_j|$, two particles interact with a one-sided harmonic contact potential, $U(r_{ij}) = \frac{1}{2}k_e(1-r_{ij}/d_{ij})^2$, whenever their separation $r_{ij} < d_{ij} = (d_i + d_j)/2$. The elastic force on i , due to contact with j , is thus $\mathbf{f}_{ij}^{\text{el}} = -dU(r_{ij})/d\mathbf{r}_i$, and the total elastic force on i is $\mathbf{f}_i^{\text{el}} = \sum_j \mathbf{f}_{ij}^{\text{el}}$, where the sum is over all j in contact with i . Particles also experience a dissipative drag force $\mathbf{f}_i^{\text{dis}}$ with respect to a suspending host medium. We take $\mathbf{f}_i^{\text{dis}} = -k_d V_i [\mathbf{v}_i - \mathbf{v}_{\text{host}}(\mathbf{r}_i)]$, where V_i is the volume of particle i and $\mathbf{v}_i = d\mathbf{r}_i/dt$. For uniform compression we define the local velocity of the host medium as $\mathbf{v}_{\text{host}}(\mathbf{r}) = -\dot{\gamma}\mathbf{r}$. This simple model has been widely used for sheared systems [6, 7, 9, 14, 26–29, 31]. Particles obey the equation of motion, $m_i[d\mathbf{v}_i/dt] = \mathbf{f}_i^{\text{el}} + \mathbf{f}_i^{\text{dis}}$, where m_i is the mass of particle i , which we take proportional to its volume V_i .

To simulate our model we use dimensionless units of length, energy, and time so that $d_s = 1$, $k_e = 1$, and $t_0 = (D/2)k_d V_s d_s^2/k_e = 1$, where $D = 2, 3$ is the dimensionality of the system. We define the quality factor $Q \equiv \tau_d/\tau_e = \sqrt{m_s k_e}/k_d V_s d_s$ as the ratio of the dissipative time $\tau_d = m_s/(k_d V_s)$ and the elastic time $\tau_e = \sqrt{m_s d_s^2/k_e}$ [25]. We set the mass of the small particles m_s so that $Q = 0.01$ in 2D and 0.0225 in 3D, which puts our system in the strongly overdamped limit $Q < 1$ [25]. We use LAMMPS [32] to integrate the equations of motion, using a time step of $\Delta t/t_0 = 0.01$. Our system consists of N particles in a cubic (square) box of length L . We perform compression by decreasing the box length at a fixed strain rate, $dL/dt = -\dot{\gamma}L$, while the particles are acted on by the compressing host medium via the above $\mathbf{f}_i^{\text{dis}}$. This results in an increasing packing fraction $\phi = N(V_s + V_b)/(2L^D)$. We take periodic boundary conditions in all directions. Compressing our system at rates from $\dot{\gamma} = 10^{-5}$ down to $10^{-8.5}$ we measure the pressure from the elastic forces, $p = L^{-D} \sum_{i < j} \mathbf{f}_{ij}^{\text{el}} \otimes (\mathbf{r}_i - \mathbf{r}_j)$, as a function of the packing ϕ . To check for finite size effects, we compare systems with $N = 16384$ and $N = 32768$ particles, averaging over 10 independent random initial

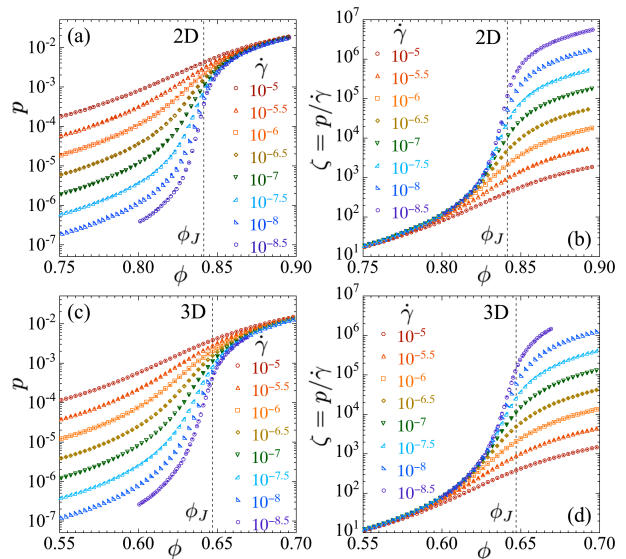


FIG. 1. (a) Pressure p and (b) bulk viscosity $\zeta = p/\dot{\gamma}$ vs packing ϕ , for different compression rates $\dot{\gamma}$ in two dimensions, and (c) p and (d) ζ in three dimensions. The vertical dashed lines locate the jamming ϕ_J . Results for $N = 16384$ particles are shown as open symbols, while results for $N = 32768$ are solid symbols. No dependence on N is observed. Error bars are roughly the size of the data symbols.

configurations for each size. Further details of our compression protocol can be found in our supplemental material [33].

Results: In Fig. 1 we plot our results for pressure p and bulk viscosity $\zeta = p/\dot{\gamma}$ in both 2D and 3D. No finite size effect is observed in our data (see our supplemental material [33] for further details). Our results are qualitatively similar to results seen for pressure and shear viscosity in shear-driven jamming [7, 8]. From the trends observed as $\dot{\gamma} \rightarrow 0$: below ϕ_J , p vanishes while ζ approaches a constant; above ϕ_J , p stays finite while ζ diverges. As $\phi \rightarrow \phi_J$ from above, p vanishes continuously; as $\phi \rightarrow \phi_J$ from below, ζ diverges continuously, demonstrating the existence of a diverging time scale in compression-driven jamming. This is our first key result.

To confirm the above behavior, we posit that pressure obeys a critical scaling equation of the same form found in shear-driven jamming [6–9, 29],

$$p = \dot{\gamma}^q f(\delta\phi/\dot{\gamma}^{1/z\nu}), \quad \delta\phi \equiv \phi - \phi_J \quad (1)$$

where $f(x)$ is an unknown scaling function. Since we observe that $\zeta = p/\dot{\gamma}$ approaches a finite limit as $\dot{\gamma} \rightarrow 0$ below ϕ_J , Eq. (1) implies that $f(x \rightarrow -\infty) \sim |x|^{-(1-q)z\nu}$, so that for $\phi < \phi_J$,

$$\lim_{\dot{\gamma} \rightarrow 0} \zeta \sim |\phi - \phi_J|^{-\beta}, \quad \beta = (1-q)z\nu. \quad (2)$$

Above ϕ_J , we observe that p approaches a finite limit as $\dot{\gamma} \rightarrow 0$, so Eq. (1) implies that $f(x \rightarrow +\infty) \sim x^{qz\nu}$, so

that for $\phi < \phi_J$,

$$\lim_{\dot{\gamma} \rightarrow 0} p \sim (\phi - \phi_J)^y, \quad y = qz\nu \quad (3)$$

Since we find no finite size dependence in our data, we average the results from our $N = 16384$ and 32768 systems together, so as to improve our statistics. Expanding the log of the scaling function as a 5th order polynomial, $\ln f(x) = \sum_{n=0}^5 c_n x^n$, we fit our data to Eq. (1), regarding ϕ_J , q , $1/z\nu$ and the c_n as free fitting parameters.

The scaling form (1) holds only asymptotically close to the critical point, i.e., $\phi \rightarrow \phi_J$, $\dot{\gamma} \rightarrow 0$. To test that our fits are stable and self consistent, we fit to Eq. (1) using different windows of data, with $\phi \in [\phi_{\min}, \phi_{\max}]$ and $\dot{\gamma} \leq \dot{\gamma}_{\max}$, to see how our fitted parameters vary as we shrink the data window closer to the critical point. Since our polynomial expansion for the scaling function $f(x)$ should be good only for small x , we also restrict the data used in the fit to satisfy $|x| \leq 1$.

In Fig. 2 we show the results from such fits, comparing 2D and 3D systems. In Fig. 2(a) we show the jamming ϕ_J , in 2(b) the exponent β , in 2(c) the exponent y , and in 2(d) the χ^2/n_f of the fit, where n_f is the number of degrees of freedom of the fit. All quantities are plotted vs $\dot{\gamma}_{\max}$ for three different ranges of $[\phi_{\min}, \phi_{\max}]$. We use the jackknife method to estimate errors (one standard deviation statistical error) and bias-corrected averages of these parameters. We see that the fitted parameters remain constant, within the estimated errors, as $\dot{\gamma}_{\max}$ decreases and we vary the range of ϕ . This suggests that our fits are indeed stable and self consistent, and that there is no need for us to include corrections-to-scaling in the analysis, such as has been found to be necessary for simple shearing [7, 8]. The χ^2/n_f decrease as we narrow the window closer to the critical point, and for our narrowest window in ϕ the χ^2/n_f remain roughly constant at the two smallest $\dot{\gamma}_{\max}$; this is another indication of the good quality of our fits. It is difficult, however, to assess the significance of the numerical value of χ^2/n_f ; unlike for shearing, where each data point $(\phi, \dot{\gamma})$ represents an average over a steady-state shearing ensemble that is independent of its starting configuration [2], for compression the configuration at a given $(\phi, \dot{\gamma})$ is in general strongly correlated with the configuration at the previous compression step $(\phi - \Delta\phi, \dot{\gamma})$, and so the estimated errors on the data points are similarly correlated.

From Fig. 2, we see that the exponents β and y seem clearly different comparing 2D with 3D, in agreement with recent results for simple shearing [34]. Thus jamming criticality in 2D seems to be different from that in 3D. This is our second key result. Taking the fit for the narrowest range $[\phi_{\min}, \phi_{\max}]$ and $\dot{\gamma}_{\max} = 10^{-6.5}$ as representative, we use those parameters to make a scaling collapse of our data in Fig. 3, plotting $p/\dot{\gamma}^q$ vs $(\phi - \phi_J)/\dot{\gamma}^{1/z\nu}$. We see an excellent data collapse, that extends well outside the data window that was

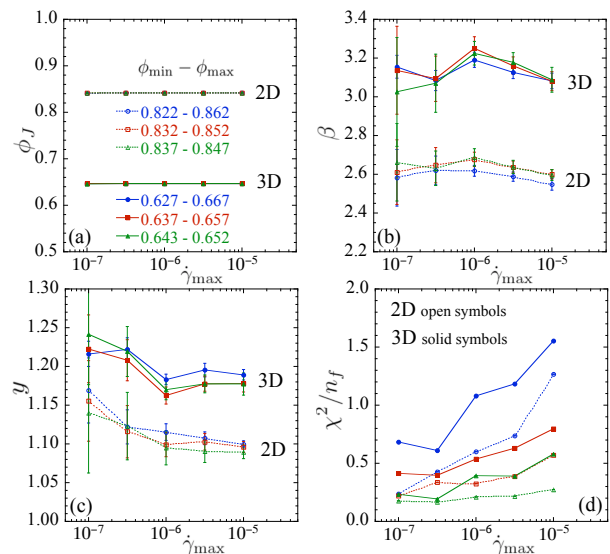


FIG. 2. Critical scaling parameters (a) ϕ_J , (b) β , (c) y , and (d) the χ^2/n_f of the fits, vs the upper limit of compression rate $\dot{\gamma}_{\max}$ used in the fit, for three different ranges of $\phi \in [\phi_{\min}, \phi_{\max}]$. Each panel shows results for both 2D and 3D systems. We use the jackknife method to compute the estimated errors and bias-corrected averages of the fit parameters. The data symbols in all panels follow the legend shown in (a); open symbols and dotted lines are for 2D, solid symbols and solid lines are for 3D.

use to determine the fit parameters. However, when $\delta\phi/\dot{\gamma}^{1/z\nu} \lesssim -2$, we see that the data depart from a common scaling curve at the larger values of $\dot{\gamma}$. We believe this is due to the effect of corrections-to-scaling that become more significant as $\dot{\gamma}$ increases and one goes further from the critical point.

Using our fit from $\dot{\gamma}_{\max} = 10^{-6.5}$ and the narrowest range of $[\phi_{\min}, \phi_{\max}]$ we find the following values of the critical parameters. In 2D we have, $\phi_J = 0.8415 \pm 0.0003$, $\beta = 2.63 \pm 0.09$, and $y = 1.12 \pm 0.04$. We can compare these to the values found in simple shearing, in which case β is the exponent associated with the divergence of the pressure analog of the shear viscosity, $\eta_p = p/\dot{\gamma}$. For shearing of the same model system as considered here, Ref. [7] gives $\phi_J = 0.8435 \pm 0.0002$, $\beta = 2.77 \pm 0.20$, and $y = 1.08 \pm 0.03$, while Ref. [9] gives $\phi_J = 0.8433 \pm 0.0001$, $\beta = 2.58 \pm 0.10$, and $y = 1.09 \pm 0.01$. We thus find that the values of the exponents β and y , found here for compression-driven jamming, agree completely, within the estimated errors, with those found for simple shearing. In 2D, compression-driven and shear-driven jamming appear to be in the same universality class. This is our third key result.

Note, our ϕ_J for compression-driven jamming is slightly lower than that found for shear-driven jamming. It is well known [2] that the value of ϕ_J can depend on the jamming protocol, and that the isotropic jamming ϕ_J found from rapid quenches of random initial con-

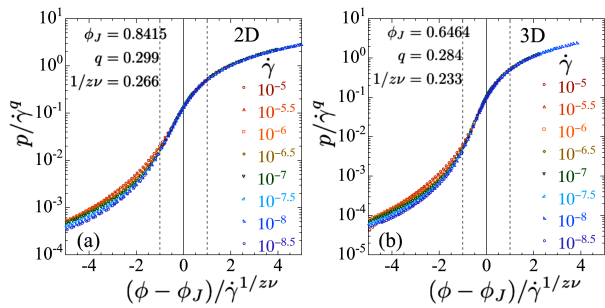


FIG. 3. Scaling collapses showing p/γ vs $(\phi - \phi_J)/\gamma^{1/z\nu}$ for (a) our 2D system, and (b) our 3D system. The values of ϕ_J , q , and $1/z\nu$ used in making these plots come from our fits for $\dot{\gamma}_{\max} = 10^{-6.5}$ and the narrowest range of $[\phi_{\min}, \phi_{\max}]$. The points within this data window, that are used to make the fit, are shown as solid symbols; the points that are not used in the fit are shown as open symbols. We see a good collapse even for data that lies well outside the data window used in the fit. The vertical solid line locates the jamming $\delta\phi = 0$; the vertical dashed lines denote the additional constraint $|x| \leq 1$ for data used in the fit.

figurations is lower than that found from shear-driven jamming. We can compare our ϕ_J for compression-driven jamming with previous values for isotropic rapid quenches. In Ref. [35], O’Hern et al. find $\phi_J = 0.842$, while in Ref. [5] Våberg et al. find 0.84177 ± 0.00001 . Both agree, within the estimated errors, with our compression-driven value above.

For our 3D system we find, $\phi_J = 0.6464 \pm 0.0005$, $\beta = 3.07 \pm 0.15$, and $y = 1.22 \pm 0.03$. Our value of ϕ_J is in reasonable agreement with the $\phi_J = 0.648$ found for the same model with the rapid quench protocol [35], and the $\phi_J = 0.6481$ found by Chaudhuri et al. [4] for a more complicated isotropic compression/decompression protocol that starts at a low ϕ_{init} ; neither of these works give an estimate for the error in their values. As in 2D, our 3D compression-driven value of ϕ_J is slightly lower than values found for simple shearing of the same model, $\phi_J = 0.6474$ in [6] and [31], and $\phi_J = 0.6491 \pm 0.0001$ in [34].

Concerning the critical exponents in 3D models of overdamped sheared suspensions, numerical simulations on hard-core spheres by Lerner et al. [6] find $\beta = 1/0.34 = 2.94$, while a later work of the same group, DeGiuli et al. [7], find $\beta = 1/0.36 = 2.8$. Simulations on soft-core spheres by Kawaski et al. [31] find $\beta = 1/0.391 = 2.56$. If one accepts the argument that $\eta_p \sim \tau$, with τ the relaxation time below ϕ_J to an unjammed configuration [8, 19], then the results of Ikeda et al. [19] give $\beta = 3.2$. None of these works discuss the exponent y . More recent work by Olsson [34], using a detailed scaling analysis including corrections-to-scaling, finds $\beta = 3.8 \pm 0.1$ and $y = 1.16 \pm 0.01$. Olsson has argued that other works find a smaller value of β because they do not probe close enough to the critical point. Given the disagreement among these

values of β for 3D simple shearing, our value of $\beta \approx 3.1$ for compression-driven jamming could be consistent with a common universality class. The situation remains to be clarified.

Note, the values of y that we find for compression-driven jamming are comparable to the values found in shear-driven jamming. Our result that $y > 1$ for compression in both 2D and 3D is surprising since it has generally been believed that $y = 1$ for our harmonic contact interaction [3, 4].

The above results were obtained by averaging together independent runs at constant values of the packing ϕ . In our supplemental material [33] we repeat our scaling analysis, but averaging our runs at constant values of the average particle contact number Z . We find no difference in any of the critical parameters between these two methods of averaging.

To summarize, we have carried out simulations of compression-driven jamming in a model of frictionless soft-core spheres in suspension, in two and three dimensions. Using the compression rate $\dot{\gamma}$ as a scaling variable, in addition to the distance to jamming $\delta\phi$, we find that the pressure, and hence the bulk viscosity ζ , obey a critical scaling law (1) of the same form as found previously for shear-driven jamming. A diverging ζ demonstrates that compression is characterized by a time scale that diverges as $\phi \rightarrow \phi_J$ from below. Unlike the claims in [1] for the relaxation time τ , we observe no finite size effects in the bulk viscosity ζ for the entire range of ϕ and $\dot{\gamma}$ we have used. Our results indicate that isotropic, compression-driven, jamming in 2D and 3D have different critical exponents. For 2D our results suggest that stress-isotropic, compression-driven, jamming is in the same universality class as stress-anisotropic, shear-driven, jamming. For 3D the situation is less clear, but our results could also be consistent with a common universality class.

We thank P. Olsson, T. A. Marschall, and M. A. Moore for helpful discussions. This work was supported by National Science Foundation Grant DMR-1809318. Computations were carried out at the Center for Integrated Research Computing at the University of Rochester.

-
- [1] A. J. Liu and S. R. Nagel, The jamming transition and the marginally jammed solid, *Annu. Rev. Condens. Matter Phys.* **1**, 347 (2010).
 - [2] C. S. O’Hern, L. E. Silbert, A. J. Liu, and S. R. Nagel, Jamming at zero temperature and zero applied stress: The epitome of disorder, *Phys. Rev. E* **68**, 011306 (2003).
 - [3] M. Wyart, L. E. Silbert, S. R. Nagel, and T. A. Witten, Effects of compression on the vibrational modes of marginally jammed solids, *Phys. Rev. E* **72**, 051306 (2005).
 - [4] P. Chaudhuri, L. Berthier, and S. Sastry, Jamming transitions in amorphous packings of frictionless spheres occur

- over a continuous range of volume fractions, *Phys. Rev. Lett.* **104**, 165701 (2010).
- [5] D. Vågberg, P. Olsson, and S. Teitel, Glassiness, rigidity, and jamming of frictionless soft core disks, *Phys. Rev. E* **83**, 031307 (2011).
- [6] P. Olsson and S. Teitel, Critical scaling of shear viscosity at the jamming transition, *Phys. Rev. Lett.* **99**, 178001 (2007).
- [7] P. Olsson and S. Teitel, Critical scaling of shearing rheology at the jamming transition of soft-core frictionless disks, *Phys. Rev. E* **83**, 030302(R) (2011).
- [8] D. Vågberg, P. Olsson, and S. Teitel, Critical scaling of Bagnold rheology at the jamming transition of frictionless two-dimensional disks, *Phys. Rev. E* **93**, 052902 (2016).
- [9] P. Olsson and S. Teitel, Herschel-Bulkley shearing rheology near the athermal jamming transition, *Phys. Rev. Lett.* **109**, 108001 (2012).
- [10] T. Hatano, Scaling properties of granular rheology near the jamming transition, *J. Phys. Soc. Jpn.* **77**, 123002 (2008).
- [11] T. Hatano, Growing length and time scales in a suspension of athermal particles, *Phys. Rev. E* **79**, 050301(R) (2009).
- [12] T. Hatano, Critical scaling of granular rheology, *Prog. Theor. Phys. Suppl.* **184**, 143 (2010).
- [13] M. Otsuki and H. Hayakawa, Critical behaviors of sheared frictionless granular materials near the jamming transition, *Phys. Rev. E* **80**, 011308 (2009).
- [14] C. Heussinger and J.-L. Barrat, Jamming transition as probed by quasistatic shear flow, *Phys. Rev. Lett.* **102**, 218303 (2009).
- [15] C. Heussinger, P. Chaudhuri, and J.-L. Barrat, Fluctuations and correlations during the shear flow of elastic particles near the jamming transition, *Soft Matter* **6**, 3050 (2010).
- [16] P. Urbani and F. Zamponi, Shear Yielding and Shear Jamming of Dense Hard Sphere Glasses, *Phys. Rev. Lett.* **118**, 038001 (2017).
- [17] Y. Jin, P. Urbani, F. Zamponi, H. Yoshino, A stability-reversibility map unifies elasticity, plasticity, yielding, and jamming in hard sphere glasses, *Sci. Adv.* **4**: eaat6387 (2018).
- [18] Y. Jin and H. Yoshino, A jamming plane of sphere packings, arXiv:2003.10814 (2020).
- [19] A. Ikeda, T. Kawasaki, L. Berthier, K. Saitoh, and T. Hatano, Universal relaxation dynamics of sphere packings below jamming, *Phys. Rev. Lett.* **124**, 058001 (2020).
- [20] E. Lerner, G. Düring, and M. Wyart, A Unified framework for non-Brownian suspension flows and soft amorphous solids, *Proc. Natl. Acad. Sci. U.S.A.* **109**, 4798 (2012).
- [21] P. Olsson, Relaxation times and rheology in dense athermal suspensions, *Phys. Rev. E* **91**, 062209 (2015).
- [22] Y. Nishikawa, A. Ikeda, and L. Berthier, Relaxation dynamics of non-Brownian spheres below jamming, arXiv:2007.09418 (2020).
- [23] A. Donev, F. H. Stillinger, and S. Torquato, Do Binary Hard Disks Exhibit an Ideal Glass Transition?, *Phys. Rev. Lett.* **96**, 225502 (2006).
- [24] F. Stillinger and S. Torquato, Configurational entropy of binary hard-disk glasses: Nonexistence of an ideal glass transition, *J. Chem. Phys.* **127**, 124509 (2007).
- [25] D. Vågberg, P. Olsson, and S. Teitel, Dissipation and rheology of sheared soft-core frictionless disks below jamming, *Phys. Rev. Lett.* **112**, 208303 (2014).
- [26] D. J. Durian, Foam mechanics at the bubble scale, *Phys. Rev. Lett.* **75**, 4780 (1995) and Bubble-scale model of foam mechanics: Melting, nonlinear behavior, and avalanches, *Phys. Rev. E* **55**, 1739 (1997).
- [27] S. Tewari, D. Schiemann, D. J. Durian, C. M. Knobler, S. A. Langer, and A. J. Liu, Statistics of shear-induced rearrangements in a two-dimensional model foam, *Phys. Rev. E* **60**, 4385 (1999).
- [28] B. Andreotti, J.-L. Barrat, and C. Heussinger, Shear flow of non-brownian suspensions close to jamming, *Phys. Rev. Lett.* **109**, 105901 (2012).
- [29] D. Vågberg, P. Olsson, and S. Teitel, Universality of jamming criticality in overdamped shear-driven frictionless disks, *Phys. Rev. Lett.* **113**, 148002 (2014).
- [30] E. DeGiuli, G. Düring, E. Lerner, and M. Wyart, Unified theory of inertial granular flows and non-Brownian suspensions, *Phys. Rev. E* **91**, 062206 (2015).
- [31] T. Kawasaki, D. Coslovich, A. Ikeda, and L. Berthier, Diverging viscosity and soft granular rheology in non-Brownian suspensions, *Phys. Rev. E* **91**, 012203 (2015).
- [32] See: <https://lammmps.sandia.gov/>
- [33] Supplemental Material at [URL] discusses details of our compression protocol, tests for the absence of finite size effects, the fluctuations between different independent compression runs, and results when we average samples at constant average contact number Z , rather than at constant packing ϕ .
- [34] P. Olsson, Dimensionality and viscosity exponent in shear-driven jamming, *Phys. Rev. Lett.* **122**, 108003 (2019).
- [35] C. S. O'Hern, S. A. Langer, A. J. Liu, and S. R. Nagel, Random Packings of Frictionless Particles, *Phys. Rev. Lett.* **88**, 075507 (2002).
- [36] P. Chaudhuri, L. Berthier, and S. Sastry, Jamming Transitions in Amorphous Packings of Frictionless Spheres Occur over a Continuous Range of Volume Fractions, *Phys. Rev. Lett.* **104**, 165701 (2010).
- [37] D. Vågberg, D. Valdez-Balderas, M. A. Moore, and P. Olsson and S. Teitel, "Finite-size scaling at the jamming transition: Corrections to scaling and the correlation-length critical exponent," *Phys. Rev. E* **83**, 030303(R) (2011)

Critical Scaling of Compression-Driven Jamming of Frictionless Spheres

Supplemental Material

COMPRESSION PROTOCOL

To initiate our simulations, we start with configurations of randomly positioned particles at a small packing fraction ϕ_{init} . To remove the large unphysical particle overlaps present in such configurations, we relax them towards a zero energy state, using our equations of motion without compression ($\dot{\gamma} = 0$). We then continue the simulations, compressing at a finite rate $\dot{\gamma}$ as described in the main text. We find that the pressure p , as one approaches the jamming ϕ_J , is independent of the starting ϕ_{init} , provided ϕ_{init} was taken sufficiently small.

To verify this, we performed test runs in 2D, starting with different values of $\phi_{\text{init}} = 0.3 - 0.8$, with a small system size of $N = 1024$ particles compressed at a fixed rate $\dot{\gamma} = 10^{-7}$. In Fig. SM-1(a) we plot the resulting pressure p vs packing ϕ . We see that $p(\phi)$ does depend on the value of ϕ_{init} at the early stages of compression. However, as the system compresses and ϕ increases, the curves for different ϕ_{init} approach a common limiting curve. Since, for our critical scaling analysis, we are only interested in behavior near jamming, for the 2D simulations described in the main text we chose $\phi_{\text{init}} = 0.4$. Fig. SM-1(a) shows that this is small enough to remove all effects of the specific value of ϕ_{init} on the values of p for $\phi \gtrsim 0.8$. For our 3D system we chose $\phi_{\text{init}} = 0.2$. Note, in Fig. SM-1(a) we also show as the open black squares our results for the $N = 32768$ system that was used in the main text. We see that these agree perfectly with the data from the smaller $N = 1024$, indicating that the desired value of ϕ_{init} does not depend on N .

For the large system sizes $N = 16384$ and 32768 used in the main text, starting compression from the above small ϕ_{init} becomes too time consuming at the slower compression rates, as one would spend much of the simulation time in the uninteresting region of low ϕ . To simulate more efficiently, we have adopted the following protocol. For our largest compression rate $\dot{\gamma} = 10^{-5}$ we compress from the small ϕ_{init} as described above. For the next smaller rate, however, we initiate the simulation with a configuration taken from the $\dot{\gamma} = 10^{-5}$ run at some larger $\phi'_{\text{init}} > \phi_{\text{init}}$. This configuration is then compressed at the smaller rate $\dot{\gamma}$. Provided ϕ'_{init} is small enough to be in the linear rheology regime where $p/\dot{\gamma}$ is independent of $\dot{\gamma}$, we find that the pressure in the initial configuration taken from the $\dot{\gamma} = 10^{-5}$ run rapidly drops to the value appropriate for the smaller rate, and then follows a smooth curve that is independent of the value of ϕ'_{init} . We use the same algorithm for each successive $\dot{\gamma}$, initializing the run from the previous larger rate, using

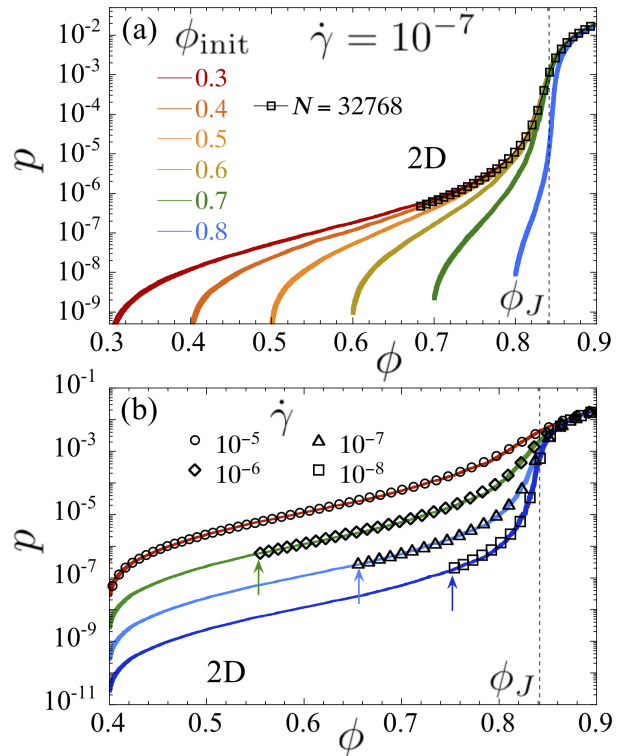


FIG. SM-1. (a) Pressure p vs packing ϕ for a 2D system with $N = 1024$ particles, at compression rate $\dot{\gamma} = 10^{-7}$. The different solid curves represent compression runs starting from different $\phi_{\text{init}} = 0.3 - 0.8$. We see that the value of $p(\phi)$ becomes independent of ϕ_{init} as ϕ increases towards jamming. The open black squares are results from the $N = 32768$ system used in the main text. We see perfect agreement with the smaller system size. (b) Pressure p vs packing ϕ for a 2D system compressed at rates $\dot{\gamma} = 10^{-5} - 10^{-8}$. The solid curves are for a system with $N = 1024$ particles, all starting from random configurations at the common $\phi_{\text{init}} = 0.4$. The larger symbols represent data from the $N = 16384$ system used in the main text, where compression starts from a larger ϕ'_{init} (indicated by the arrows) using a configuration from a run with a larger $\dot{\gamma}$. We see perfect agreement between the two data sets. In both panels, results are averaged over 10 independent initial configurations. The width of each solid curve represents the estimated error. Vertical dashed lines locate the jamming ϕ_J .

increasing values of ϕ'_{init} as $\dot{\gamma}$ decreases.

To validate this protocol, we performed test runs in 2D with $N = 1024$ particles, compressing with rates $\dot{\gamma} = 10^{-5} - 10^{-8}$, all starting from the same $\phi_{\text{init}} = 0.4$. In Fig. SM-1(b) we plot (solid lines) the resulting pressure p vs packing ϕ . On the same plot we indicate with larger symbols our results from the $N = 16384$ system used in

the main text, where compression takes place using the above described protocol. These latter runs are initiated at larger values of ϕ'_{init} , varying according to the value of $\dot{\gamma}$, as indicated by the arrows in the figure. For all $\dot{\gamma}$ we find perfect agreement between these values of $p(\phi)$ and those of the smaller system that started from the common ϕ_{init} .

FINITE SIZE EFFECTS

Since we wish our analysis to be representative of behavior in the limit of an infinite sized system, it is important to demonstrate that our data do not suffer from effects due to the finite size of our numerical system. Our results in Fig. SM-1 clearly show that there are no finite size effects at small values of ϕ . However we still need to check that there are no finite size effects near jamming. For a continuous phase transition, such as is frictionless jamming, one expects there to be a correlation length ξ that diverges as the critical point is approached. Once one has $\xi \gtrsim L/2$, with L the length of the numerical system, effects of the finite size of the system will appear. We want, therefore, to check that our system is large enough for all our data points $(\phi, \dot{\gamma})$ that they suffer from no such finite size effects.

Here we have simulated two different system sizes with $N = 16384$ and $N = 32768$ total particles. We will denote the pressure in the first case p_{16} and in the second case p_{32} . In Fig. SM-2 we plot the relative difference in pressure between these two different sized systems, $\Delta p/p \equiv 2(p_{16} - p_{32})/(p_{16} + p_{32})$, as a function of the particle packing ϕ , for our three smallest compression rates $\dot{\gamma}$. In Fig. SM-2(a) we show results for the average pressure (averaged over our 10 independent compression runs) for our 2D system; in SM-2(b) we show the corresponding results for our 3D system. The error bars represent one standard deviate of estimated statistical error. Note, the results for each $\dot{\gamma}$ are displaced vertically an amount 0.5 from the next smaller $\dot{\gamma}$, so that one can easily distinguish the different data sets. One sees that $\Delta p/p$ fluctuates about zero, and all data points are within two standard deviations of zero. This indicates that there are no systematic differences between the two system sizes, and that the finite $\Delta p/p$ is a consequence of statistical fluctuations in our finite sampling. Not surprisingly, these fluctuations are largest when one gets close to ϕ_J .

To further illustrate that the observed $\Delta p/p$ is due to statistical fluctuations and is not any systematic effect, in Figs. SM-2(c) and SM-2(d) we plot $\Delta p/p$ for our 2D and 3D systems, but now computing the pressure difference between individual samples of the two system sizes, rather than the average over all samples. We show results for six different pairs of samples. The data for each $\dot{\gamma}$ is displaced vertically an amount 1.0 from the next smaller

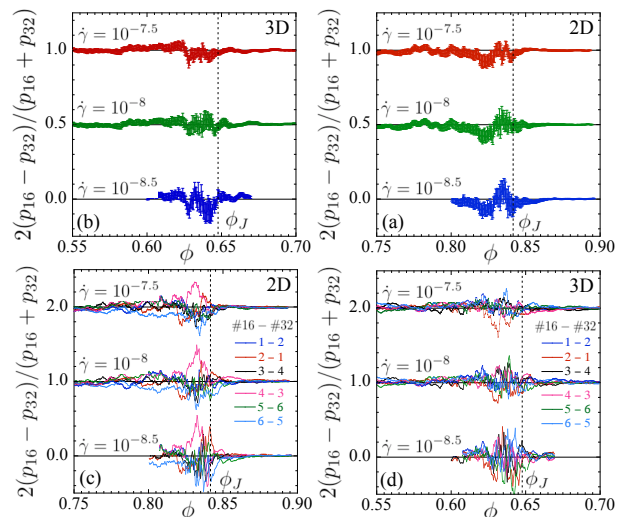


FIG. SM-2. Relative difference of pressure p_{16} of a system with $N = 16384$ particles compared to the pressure p_{32} of a system with $N = 32768$ particles. We plot $\Delta p/p \equiv 2(p_{16} - p_{32})/(p_{16} + p_{32})$ vs ϕ , showing results for our three smallest compression rates $\dot{\gamma}$. Data for different $\dot{\gamma}$ are displaced vertically so as to easily distinguish the different data sets; all are fluctuating about zero. (a) and (b) show the difference in the pressure averaged over all 10 independent compression runs for 2D and 3D systems; (c) and (d) show the difference in pressure for six different pairs of individual samples from the two system sizes. The legend “#16 – #32” indicates which sample from the smaller system is compared with which sample from the larger system. The vertical dashed lines indicate the location of the jamming ϕ_J .

$\dot{\gamma}$, so that one can easily distinguish the different data sets. Now we see that the sign of the fluctuation of $\Delta p/p$ about zero varies randomly from one configuration pair to another. Moreover, comparing the magnitude of the fluctuation of $\Delta p/p$ for the individual samples compared to the average over all samples, the latter is smaller by roughly the factor $1/\sqrt{N_s}$ (with $N_s = 10$ the number of samples) that one would expect from statistical averaging. We thus conclude that any difference we see comparing p_{16} to p_{32} is a statistical effect of finite sampling, rather than a systematic finite size effect.

We also note that we see no finite size effect in p , and hence in $\zeta = p/\dot{\gamma}$, even for the lower values of $\phi \lesssim 0.83$ in 2D, or $\phi \lesssim 0.57$ in 3D, where [1] reports finding a $\log N$ dependence of the decay time τ to relax to an unjammed state for systems of our size. Thus, whatever is the dependence of τ on N , there does not seem any corresponding effect for ζ .

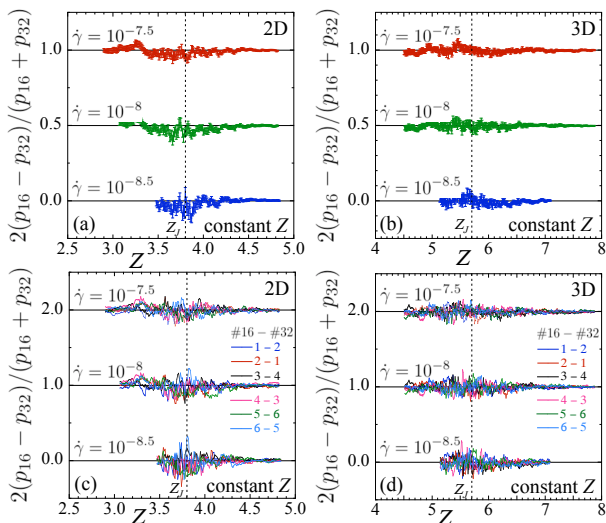


FIG. SM-3. Relative difference of pressure p_{16} of a system with $N = 16384$ particles compared to the pressure p_{32} of a system with $N = 32768$ particles. We plot $\Delta p/p \equiv 2(p_{16} - p_{32})/(p_{16} + p_{32})$ vs Z , showing results for our three smallest compression rates $\dot{\gamma}$. Data for different $\dot{\gamma}$ are displaced vertically so as to easily distinguish the different data sets; all are fluctuating about zero. (a) and (b) show the difference in the pressure averaged at constant Z over all 10 independent compression runs for 2D and 3D systems; (c) and (d) show the difference in pressure for six different pairs of individual samples from the two system sizes. The legend “#16 - #32” indicates which sample from the smaller system is compared with which sample from the larger system. The vertical dashed lines indicate the location of the jamming Z_J .

AVERAGING AT CONSTANT CONTACT NUMBER Z

In the main text of this paper we have averaged our independent samples together at constant values of the system packing ϕ . One may wonder if this is the best thing to do for the following considerations. For a simple sheared system, when the system is sheared for a sufficiently long time, the average over the ensemble of sheared steady-state configurations becomes independent of the initial starting configuration [2]. Statistical fluctuations in the data at a given $(\phi, \dot{\gamma})$ are thus, in principle, independent of the fluctuations in the data at other $(\phi, \dot{\gamma})$.

For compression, however, the configuration at a given step $(\phi, \dot{\gamma})$ is strongly correlated with the configuration at the previous step $(\phi - \Delta\phi, \dot{\gamma})$. It was found that the jamming point ϕ_{Ji} , where a configuration first develops a finite pressure p , can depend on the particular initial configuration i from which the compression started [3, 4]. For a system with a finite number of particles N , there will thus be a spread $\Delta\phi_J$ in these ϕ_{Ji} . This spread $\Delta\phi_J \rightarrow 0$ as $N \rightarrow \infty$ [3, 5].

It is not clear if this behavior should affect the criti-

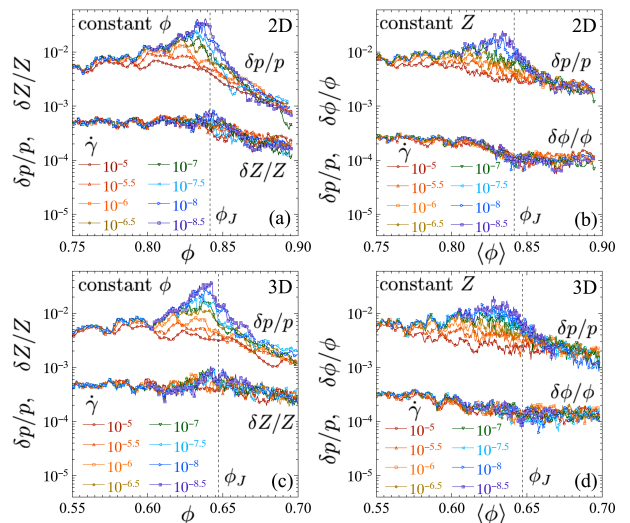


FIG. SM-4. Relative statistical errors in measured quantities for 2D and 3D systems, comparing averaging at constant ϕ with averaging at constant Z . (a) Relative errors $\delta p/p$ and $\delta Z/Z$ vs ϕ for our 2D system, when averaging at constant ϕ . (b) Relative errors $\delta p/p$ and $\delta\phi/\phi$ vs the average $\langle\phi\rangle$ for our 2D system, when averaging at constant Z . Results are shown for our different compression rates $\dot{\gamma}$. (c) and (d) show the corresponding results for our 3D system. Vertical dashed lines locate the jamming ϕ_J .

cal scaling analysis carried out in the main text of this work. We are interested in the ϕ_J that characterizes the ensemble of compression runs, rather than any individual run. We have found that the average $\langle\phi_{Ji}\rangle$ is independent of the initial configurations, if these are taken randomly at sufficiently small ϕ_{init} . However the width $\Delta\phi_J$ will be one source of fluctuation in the measured pressure, if averaging over configurations at constant ϕ . Because of this, several works [3, 4] have analyzed critical properties by averaging configurations at constant values of $(\phi - \phi_{Ji})$, rather than constant ϕ .

Alternatively, one could average configurations at constant values of the average number of contacts per particle Z [6–8]. Even though different configurations of finite size systems may jam at different ϕ_{Ji} , they all jam at the same isostatic contact number $Z_{\text{iso}} = 2d$, provided one has removed rattler particles [3] in the computation of Z . Here d is the spatial dimensionality of the system. Thus averaging at constant Z removes the effect of the variations in ϕ_{Ji} . Because the identification of rattlers is most easily accomplished for mechanically stable configurations above jamming, and our configurations are dynamically generated, and so not in mechanical equilibrium, and also include configurations below ϕ_J , we will not attempt to remove rattlers but rather we will compute the contact number Z averaged over all particles. Thus our Z_J at jamming will be slightly smaller than Z_{iso} . Nevertheless we can expect that averaging at con-

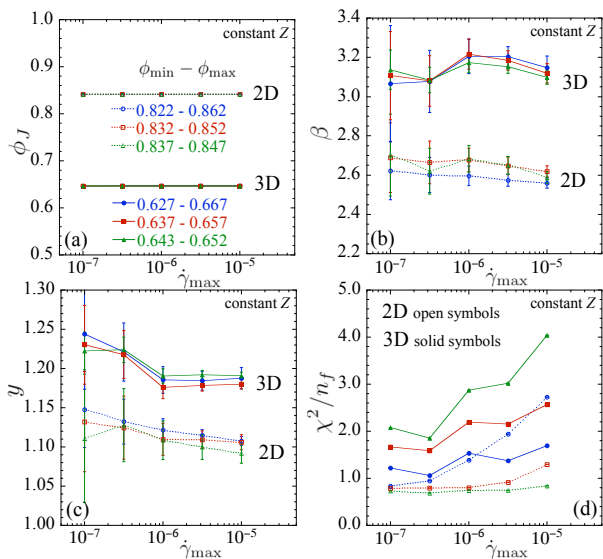


FIG. SM-5. Critical scaling parameters (a) ϕ_J , (b) β , (c) y , and (d) the χ^2/n_f of the fits, vs the upper limit of compression rate $\hat{\gamma}_{\max}$ used in the fit, for three different ranges of $\phi \in [\phi_{\min}, \phi_{\max}]$. Each panel shows results for both 2D and 3D systems. We use the jackknife method to compute the estimated errors and bias-corrected averages of the fit parameters. The data symbols in all panels follow the legend shown in (a); open symbols and dotted lines are for 2D, solid symbols and solid lines are for 3D. The results shown here come from fits to our data when we have averaged our independent compression runs at constant values of the average contact number per particle Z .

stant Z will still compensate for the variations in ϕ_{Ji} , as there should on average be a fixed fraction of rattlers at jamming. In this section we therefore repeat our analysis of the critical behavior of compression-driven jamming, but averaging our independent compression runs together at constant values of Z . In the end we will find no differences in any of the critical parameters from those found in the main text, where we averaged at constant ϕ .

First we investigate whether there are any finite size effects in our data, as we did for constant ϕ averaging, comparing systems of size $N = 16384$ and $N = 32768$. Computing $\Delta p/p$, now averaging at constant Z , we show our results in Fig. SM-3. We again see no systematic finite size effects; the observed $\Delta p/p$ is consistent with the statistical effect of finite sampling. Comparing with Fig. SM-2 it appears that these statistical fluctuations are somewhat smaller when averaging at constant Z as compared to averaging at constant ϕ , particularly near jamming. Since we find no evidence for any systematic finite size effect, in the analysis below we combine our results from the two system sizes so as to have 20 independent samples.

Next we consider the relative statistical errors in the measured quantities, comparing averaging at constant ϕ with averaging at constant Z . Since our compression runs

are independent of one another, the estimated statistical error in pressure δp is related to the standard deviation σ_p of the distribution of pressures by $\delta p = \sigma_p/\sqrt{N_s}$, where $N_s = 20$ is the number of samples. In Fig. SM-4(a) we show the relative errors $\delta p/p$ and $\delta Z/Z$ vs the packing ϕ in our 2D system, for the case where we average our configurations together at constant ϕ . We show results for our different compression rates $\hat{\gamma}$. In Fig. SM-4(b) we similarly show $\delta p/p$ and $\delta\phi/\phi$ when we average at constant Z . To make for an easier comparison, we plot these vs the average packing $\langle\phi\rangle$ rather than the fixed Z . In Fig. SM-4(c) and SM-4(d) we show the same quantities for our 3D system.

Not surprisingly, we see that the errors are largest near jamming. The errors $\delta p/p$ show a stronger variation with $\hat{\gamma}$, becoming larger as $\hat{\gamma}$ decreases, than do the errors $\delta Z/Z$ or $\delta\phi/\phi$, which are an order of magnitude or more smaller. Comparing averaging at constant ϕ to averaging at constant Z , we see that the errors in the latter case are slightly smaller near ϕ_J , as might be expected from the discussion that introduced this section. Note, however, that as we go either below or above ϕ_J , the errors when we average at constant Z become slightly larger than when we average at constant ϕ .

The reduced fluctuations between system sizes near ϕ_J seen in Fig. SM-3, and the reduced errors near ϕ_J seen in Fig. SM-4, when we average at constant Z as compared to constant ϕ , suggest that averaging at constant Z might give improved results for our scaling analysis. However we find that this is not the case. Using our values of p and ϕ , averaged over the different compression runs at constant Z , we fit to the scaling equation (1) of the main text using the same methods as described there. In Fig. SM-5 we show our results.

In Fig. SM-5(a) we show the jamming ϕ_J , in SM-5(b) the exponent β , in SM-5(c) the exponent y , and in SM-5(d) the χ^2/n_f of the fit, where n_f is the number of degrees of freedom of the fit. For all quantities we plot our results vs $\hat{\gamma}_{\max}$ for three different ranges of $[\phi_{\min}, \phi_{\max}]$. Comparing these to Fig. 2 of the main text, no appreciable difference is seen. The fits are stable and self-consistent as we vary the window of data used in the fit. Using $\hat{\gamma}_{\max} = 10^{-6.5}$ and the narrowest range of $[\phi_{\min}, \phi_{\max}]$, we find the following results. In 2D we have, $\phi_J = 0.8415 \pm 0.0004$, $\beta = 2.62 \pm 0.12$, and $y = 1.13 \pm 0.05$. In 3D we have, $\phi_J = 0.6464 \pm 0.0005$, $\beta = 3.08 \pm 0.16$ and $y = 1.22 \pm 0.04$. These are exactly the same values, within the estimated errors, as we found in the main text when averaging at constant ϕ . Moreover, the estimated errors found here are roughly the same, and in some cases a bit bigger, than we found in the main text. We conclude that, for our system sizes, there is no advantage in averaging at constant Z as compared to the simpler averaging at constant ϕ .

-
- [1] Y. Nishikawa, A. Ikeda, and L. Berthier, Relaxation dynamics of non-Brownian spheres below jamming, arXiv:2007.09418 (2020).
 - [2] D. Vågberg, P. Olsson, and S. Teitel, Glassiness, rigidity, and jamming of frictionless soft core disks, *Phys. Rev. E* **83**, 031307 (2011).
 - [3] C. S. O’Hern, L. E. Silbert, A. J. Liu, and S. R. Nagel, Jamming at zero temperature and zero applied stress: The epitome of disorder, *Phys. Rev. E* **68**, 011306 (2003).
 - [4] P. Chaudhuri, L. Berthier, and S. Sastry, Jamming Transitions in Amorphous Packings of Frictionless Spheres Occur over a Continuous Range of Volume Fractions, *Phys. Rev. Lett.* **104**, 165701 (2010).
 - [5] D. Vågberg, D. Valdez-Balderas, M. A. Moore, and P. Olsson and S. Teitel, “Finite-size scaling at the jamming transition: Corrections to scaling and the correlation-length critical exponent,” *Phys. Rev. E* **83**, 030303(R) (2011)
 - [6] E. Lerner, G. Düring, and M. Wyart, A Unified framework for non-Brownian suspension flows and soft amorphous solids, *Proc. Natl. Acad. Sci. U.S.A.* **109**, 4798 (2012).
 - [7] E. DeGiuli, G. Düring, E. Lerner, and M. Wyart, Unified theory of inertial granular flows and non-Brownian suspensions, *Phys. Rev. E* **91**, 062206 (2015).
 - [8] P. Olsson, Relaxation times and rheology in dense athermal suspensions, *Phys. Rev. E* **91**, 062209 (2015).